Ground-Penetrating Radar Simulation in Engineering and Archaeology

Article *in* Geophysics · February 1994

DOI: 10.1190/1.1443584

1 author:

Dean Goodman
University of California, Santa Barbara
71 PUBLICATIONS **1,611** CITATIONS

Ground-penetrating radar simulation in engineering and archaeology

Dean Goodman*

GEOPHYSICS, VOL. 59, NO. 2 (FEBRUARY 1994) P. 224–232, 9 FIGS.

GEOPHYSICS, VOL. 59, NO. 2 (FEBRUARY 1994) P. 224–232, 9 FIGS.

Ground-penetrating radar simulation in engineering and archaeology

Dean Goodman*

ABSTRACT

Forward modeling of ground penetration radar is developed using exact ray-tracing techniques. Structural boundaries for a ground model are incorporated via a discrete grid with interfaces described by splines, polynomials, and in the case of special structures such as circular objects, the boundaries are given in terms of their functional formula. In the synthetic radargram method, the waveform contributions of many different wave types are computed. Using a finely digitized antenna directional response function, the radar cross-section of buried targets and the effective area of the receiving antenna can be statistically modeled. Attenuation along the raypaths is also monitored. The forward models are used: (1) as a learning tool to avoid pitfalls in radargram interpretation, (2) to understand radar signatures measured across various engineering structures, and (3) to predict the response of cultural structures buried beneath important archaeological sites in Japan.

INTRODUCTION

Ground-penetrating radar (GPR) has been applied in a variety of studies including: groundwater investigations, identification of buried hazardous wastes, soils mapping, as well as engineering and geo-technical investigations (e.g., Davis and Annan, 1989; Daniels, 1988; Foster et al., 1987; Olhoeft, 1986; Ulriksen, 1982; Annan and Davis, 1976; Stewart and Unterberger, 1976). GPR has also been found to be a useful tool for nondestructive archaeological investigations (e.g., Goodman and Nishimura, 1992 and 1993; Bevan 1975, 1991; Stove and Addyman, 1989; Vaughn, 1986).

Current GPR research is concentrating on the development of equipment and software to keep pace with the needs of a growing scientific community that would like to collect and analyze data in a similar fashion to that already practiced in seismic exploration. Multichannel receivers and transmitters for collecting 3-D GPR data have recently been proposed (Deen and Feijter, 1992). An example of limited 2-D array data collection has been recently published (Fisher et al., 1992).

What can be considered the "pioneer" research in terms of GPR interpretation is the introduction of techniques similar to those found in the seismic industry including: 2-D and 3-D migration (e.g., Turner, 1992), complex wavenumber filtering, deconvolution, velocity analysis, etc. Also, commonly practiced in seismic interpretation are 2-D and 3-D forward modeling. Forward modeling can help to corroborate geologic interpretations made from raw or processed seismic data sets. Currently, however, forward GPR modeling is restricted to 1-D structures in the literature.

In this study, a method for simulating GPR returns from buried structures is developed. Some of the nomenclature used is inherently similar to that found in the seismological literature (e.g., Telford et al., 1990). There are however, some differences in modeling of GPR signals. One of the primary differences is the fact that the GPR method normally transmits and receives signals recorded over a spatial window—the antenna aperture. In the seismic method, the receivers (geophones), are normally considered to be point measurers of ground motions. The effective aperture (spatial window) of the antenna is an essential factor needed to properly predict the amplitudes of radar returns, particularly for reflectors located close to the antenna. One-dimensional synthetic radargrams have been used frequently in the literature. However, properly predicting radar signatures from 1-D structures in the ground requires higher dimensional modeling to account for the effects of antenna aperture, as well as geometric spreading.

Other factors that can distinguish microwave radiation from simple elastic seismic wave radiation are the dispersive nature of microwaves. In the case of inelastic seismic waves, however, analogies can be drawn between dispersive microwaves and seismic waves. In this study the dispersive characteristics of microwaves are not modeled, since it is

Manuscript received by the Editor July 9, 1992; revised manuscript received May 17, 1993.
*Geophysical Archaeometry Laboratory, University of Miami Japan Division, Otsubu 39-1, Nakajima Machi, Ishikawa 929-22 Japan.

assumed that a monofrequency radar impulse is transmitted into the ground. In part, there is some justification for ignoring the dispersive characteristic of microwaves given the fact that the GPR transmitted signal for many pulsed radar systems are close to, but not completely, a monofrequency signal.

A method for incorporating dispersion into the GPR modeling given in this study, however, can be easily conceived in theoretical calculation, but less so in actual computational practice. Essentially, computing the forward model at a variety of different frequencies with initial conditions given by the frequency components of the transmitted pulse, and then superposing the resultant solutions, can effectively produce forward models that incorporate microwave dispersion. A similar 1-D application is discussed by Lau et al., (1992). Dispersive 2-D and 3-D forward modeling efforts are left for future studies.

RADAR MODELING PROCEDURES

In keeping with the historical development of GPR, which evolved from airborne radar, a brief mention of the equation describing signals returned from airborne targets is presented. The radar equation of a lossy medium describes the power received from a target (Radar Handbook, 1990):

$$P_r = \frac{G_t P_t A_e C}{(4\pi)^2 R_t^2 R_r^2} \exp\left[-2a(R_t + R_r)\right],$$

where

G_t = transmitter gain
P_t = transmitted power
R_t = transmitter-target distance
R_r = receiver-target distance
a = attenuation coefficient
A_e = effective area of receiving antenna
C = target radar cross-section.

Although in principle the radar equation is a formulism derived mainly for use in flight detection problems, some of the factors that could affect GPR returns from buried targets in the ground are described: (1) the effective area of the receiving antenna, (2) target cross-sections, and (3) the signal attenuation. The purpose of forward modeling is to accurately estimate the return signal of microwaves that propagate into lossy earth media, are reflected from targets having a specified cross-section, return from the target after undergoing reflection/transmission, and intersect some effective area of the receiving antenna. In forward modeling the transmitter-target and receiver-target distances are specified according to the model structure along with transmitted power and gains.

To simulate the time-varying signal recorded with ground-penetrating radar, the following formula describing a synthetic radargram is developed:

$$S(t) = I_t(t) * I_r(t) * \sum_{\theta} D(\theta) \sum_{k} Q_k(t),$$

where

S = synthetic radar scan
I_t = transmitted impulse wavelet
I_r = receiver impulse response
D = directional response of the antenna
Q = return amplitude response for a ray that may undergo reflection, transmission, refraction, and attenuation along the path of a kth wave type
t = time.

The kth wave type refers to a set of traveling instructions for a particular ray. For example, for a kth wave type designated as "R," the raypath will include a single reflection; for a wave type given as "TRT," rays examined will first undergo a transmission, then reflection, followed by transmission across various structural boundaries, etc.

The synthetic radar scan is represented by a summation over the entire directional response of the antenna and a summation over the wave type. Different wave types are traced through the structure that has been digitized into a discrete grid. The grid cells contain a total of four parameters; three material parameters (ε-complex dielectric permittivity, σ-conductivity, μ-magnetic permeability) and one identifier P_x containing the coefficients of a spline or polynomial or a functional formula describing structural interfaces through the grid cell(s) (Figure 1). The polynomials allow for an infinite number of possible slope determinations in a single-grid cell. For this reason, the method has been referred to as the "Infinite slope method" (Goodman and Nishimura, 1992) to distinguish it from a "finite" or single-slope value within a single cell.

The advantages of describing structural slopes in terms of shape functions are that small scale structures can be digitized into a relatively coarse grid, while still preserving the entire structural/slope information. In addition, the method

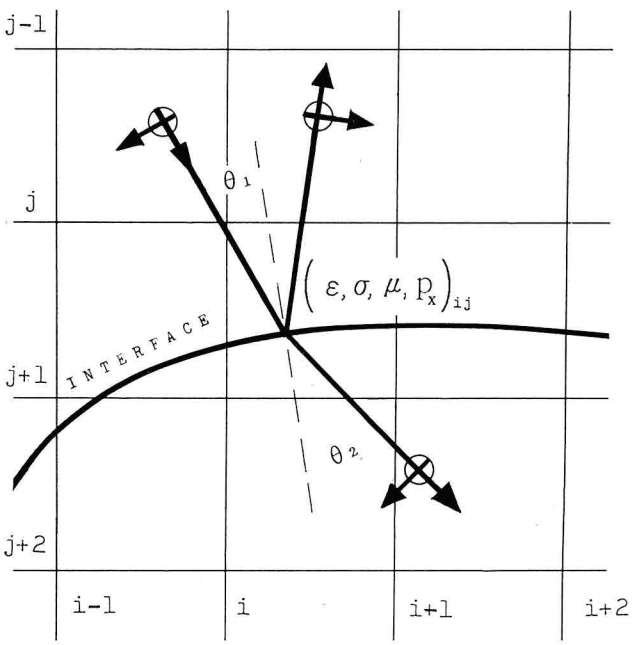

FIG. 1. A description of the discrete grid used in GPR simulations. Each grid cell contains values of dielectric permittivity, conductivity, permeability, and a shape function identifier for use in determining structural (slope) information.

is independent of the cell shape, since the grid cells are only used to identify the location of structural boundaries. The antenna aperture, although not explicitly written into the synthetic radargram formula, is incorporated into the simulation by the presence of the antenna "receiver" existing across several grid cells.

The propagation of electromagnetic waves used in the infinite slope method (ISM) can easily incorporate varying propagation models; currently a conductive-dissipative wave theory is incorporated (Jackson, 1977). The form of the governing electromagnetic wave equation for the electric field propagating in the z-direction is

$$\frac{d^2\mathbf{E}(z)}{dz^2} = \gamma^2\mathbf{E}(z).$$

The propagation vector γ has both real and imaginary parts and is defined as $(a + ib)$. The real part gives the attenuation coefficient of the electromagnetic wave. The attenuation coefficient at a discrete angular frequency ω is

$$a = \omega(\tfrac{1}{2}\mu\varepsilon'[(1 + \tan^2\delta)^{1/2} - 1])^{1/2}.$$

The imaginary part of the propagation vector, the phase constant, is

$$b = \omega(\tfrac{1}{2}\mu\varepsilon'[(1 + \tan^2\delta)^{1/2} + 1])^{1/2},$$

where $\tan\delta$, the loss tangent, is defined as

$$\tan\delta = \left[\frac{(\sigma + \omega\varepsilon'')}{\omega\varepsilon'}\right],$$

and $'$ and $''$ refer to the real and imaginary parts of the dielectric permittivity, respectively. This equation assumes that the imaginary parts of both the magnetic permeability and conductivity are taken as 0. For most materials, other than some metals, the real part of the magnetic permeability in the above equations can be approximated as the magnetic permeability in free space ($4\pi 10^{-7}$ H/m). The loss tangent gives a measure of the frequency-dependent dissipation of electromagnetic wave energy caused by dc conduction and dielectric relaxation (Duke, 1990).

The use of general optics theory to describe the reflection and transmission of electromagnetic radiation is assumed to be valid in the ISM synthetic radargram. In this case the structures considered are assumed to be larger than the wavelength of the microwave radiation. The reflection and transmission of parallel polarized microwaves is

$$R = \frac{Z_2\cos\theta_1 - Z_1\cos\theta_2}{Z_2\cos\theta_1 + Z_1\cos\theta_2};$$

$$T = \frac{2Z_2\cos\theta_1}{Z_2\cos\theta_1 + Z_1\cos\theta_2},$$

where the complex electromagnetic impedance is given by

$$Z = \sqrt{\frac{j\omega\mu}{\sigma + j\omega\varepsilon}}.$$

For those antennas that may have mixed polarization transmission properties, the perpendicular polarized wave components can also be included.

Refraction at the interface between two different materials is found from Snell's law:

$$b_1\sin\theta_1 = b_2\sin\theta_2.$$

The return amplitude response computed in the GPR radargram simulation for the kth wave type that is attenuated and undergoes reflections $(R_1, R_2 \ldots R_i)$ and transmissions $(T_1, T_2 \ldots T_j)$ is

$$Q_k(t) = A_k(R_1R_2 \ldots R_i)_k(T_1T_2 \ldots T_j)_k\delta(t - t_k),$$

where the attenuation factor along the path (ϕ) of the wave is

$$A = \int_\phi e^{-a(\phi)}\,d\phi.$$

The indices $1 \ldots i$ and $1 \ldots j$ refer to two media encountered along the raypath. The delay time of the kth ray is t_k, given by the integral of the inverse wave velocity (wave slowness) over the path of the kth wave type ray:

$$t_k = \int_\phi \frac{1}{v(\phi)}\,d\phi,$$

where the microwave phase velocity is $v = \omega/b$. With the use of the delta function, the return amplitude response contains a series of spikes. The magnitudes of the spikes correspond to the combinations of reflection and transmission coefficients along with attenuation factors for the kth wave type, with locations at time t_k.

The final process in creating the synthetic radar scan involves the convolution with the instrumentation responses including the receiving and transmitting antenna. The impulse response wavelet is normally assumed to represent a far-field response of the antenna, although near-field responses can also be used if they are known and if reflected waves are recorded within the near-field time window. Most ground radar antenna impulses approach far-field antenna responses within a half wavelength in the ground (Duke, 1990).

To start the computation of the GPR radargram, rays are sent into the grid having a direction and starting amplitude specified by the directional response (radiation pattern). The ray has a particular wave type specification indicating whether reflection and/or transmission will occur at the various boundaries encountered during its travel. If the waves return to the starting grid location or within grids representing the horizontal aperture of the antenna, then they are recorded. If the wave exceeds the time window designated, the wave is not recorded and the next wave type is started. If a wave encounters more interfaces than is specified for the kth wave type, it is also discarded.

One important point to stress about the synthetic radargram simulation is that the method incorporates and properly predicts the effects of geometrical spreading in refractive media. The relative amplitudes of features in the model can be statistically sampled and radar cross-sections esti-

mated for buried targets/structures. To successfully implement and predict geometrical spreading effects requires a proper digitization interval used to simulate the directional response of the radar antenna. For structural models in which small objects at great depth are observed, a very fine digitization interval for the response is necessary to ensure that the target is recorded. With a proper digitization interval, the full waveform of GPR signals can be predicted.

EXPERIMENTAL TEST COMPARISON

A new interactive modeling software package, GPRSIM (c. 1993, 1992) (short for *G*round *P*enetrating *R*adar *SIM*ulation) was first tested with data collected at an experimental test site (Figure 2). A 6 m × 3 m test hole was dug to a depth of 1 m. Relatively homogeneous beach sand was found from 0–60 cm, below which clay was encountered. Three cylindrical objects, a plastic pipe, a metal pipe, and a tree trunk still containing bark, were buried to 1 m, and then fresh gravely sand commonly used in road construction was used to fill the test pit.

A 500 MHz shielded antenna having the directional response function given in Figure 3, was used to collect radar reflection data within a 40 ns time window over the test site. The impulse response was estimated from reflections measured from the buried metal pipe. The test site was digitized into 2 cm × 2 cm grid cells. The directional response function was sampled every 0.1 degrees. The prediction traveltimes of two primary wave types, *R* and *RR*, are computed across the test structure (Figure 2).

The measured radargram is compared with a simulation estimated for the known test structure (Figure 2). Because of the wide field of view of the radar antenna, objects off to the side of the antenna can be recorded, resulting in hyperbolic reflection patterns, as in the case for buried cylindrical (pipe) structures. The reflection patterns of the *R* wave type show clear hyperbolic-type reflection patterns. Also, the multiple wave type *RR*, and its presence in the synthetic and measured data can be clearly seen. In particular, the corner reflection produces very strong responses in the measured and synthetic radargrams. Some secondary *RR* wave energy is also seen in at least the synthetic radargram, although it is not as clear in the measured radargram. The *RR* wave energy that appears to be almost parallel to the *R* hyperbolic reflection pattern and slightly delayed, is caused by a wave that just grazes off the cylindrical objects–hits the sand/clay interface or vice versa–and then returns to the antenna. Another secondary *RR* wave is predicted which hits the cylindrical object–bounces off the side walls of the test pit–and then is returned to the antenna. This wave type is shown to have some small but "realizable" amplitude after the recorded signals were converted to typical digital data having a dynamic range of −127 to +127.

Some adjustments to the final electromagnetic parameters used in the simulation were made during several trial runs. The final values chosen are: pit sand ($\varepsilon' = 10.5$, $\sigma = 0.001$ mho/m); beach sand ($\varepsilon' = 8$, $\sigma = 0.0001$ mho/m); clay ($\varepsilon' = 7$, $\sigma = 0.01$ mho/m); plastic pipe ($\varepsilon' = 4$, $\sigma = 0.0001$ mho/m); metal pipe ($\varepsilon' = 1$, $\sigma = 100000$ mho/m); tree trunk ($\varepsilon' = 5$, $\sigma = 0.001$ mho/m).

The test simulation shows that it is possible to predict many of the patterns recorded with GPR. The simulation also shows how different radargrams can look, as compared to the actual structures that created them. Particularly in the case of strictly vertical profiling with a GPR instrument, which is the most common form of data collection today, radargrams can be quite deceiving. Migration can accurately solve the problem of "collapsing" the hyperbolic reflection patterns; nonetheless, the multiple reflection from the corner of the test pit would still remain an unsolved mystery in piecing together the candidate test structure had it not been previously known.

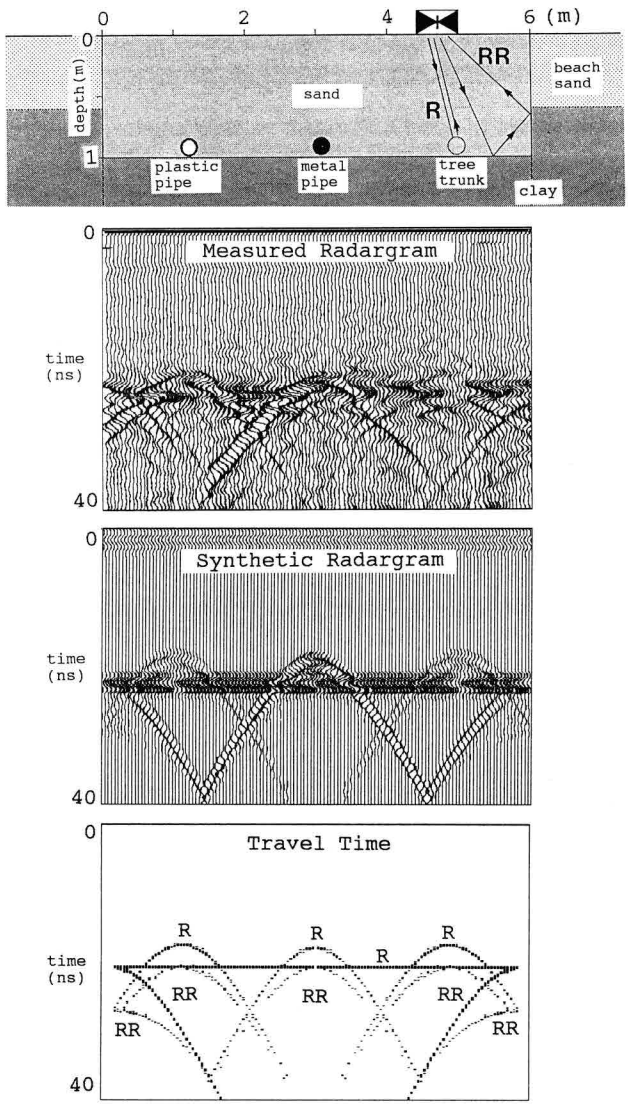

FIG. 2. A comparison of a 500 MHz measured radargram and a synthetic radargram found for an experimental test site that was built. The contributions of the primary wave types *R* and *RR* are computed. The corner reflections and reflection multiples that bounce off the cylindrical objects and the walls or the test hole floor are also predicted with the simulation software GPRSIM.

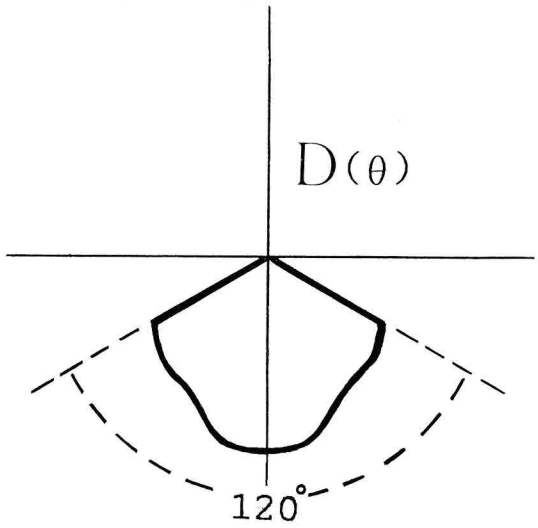

FIG. 3. The antenna directional-response function used in the simulation of GPR radargrams. The response function is adapted from a commercially available antenna (see Goodman and Nishimura, 1992).

Before a study of some engineering applications, several common radargram "pitfalls" that are useful in understanding and interpreting GPR signals are presented.

RADARGRAM PITFALLS

Analogous to "seismic pitfalls" (see, for example, Gassaway et al., 1987; Tucker and Yorston, 1973; and others), radar is also subject to similar problems of interpretation. To exemplify some of these problems, a simulation across a simple three-layer structure is computed (Figure 4). The top layer has a variable thickness; the second interface is modeled as a horizontal surface. The wave types *R*, *RRR*, *TRT*, *TRRRT*, and the wave types *TRTRR* and *RRTRT* (commonly referred to as "peg-leg" multiples in the seismic literature) are simulated across the model structures. For 1-D models the peg-leg multiples follow the same 1-D ray paths. However, for 2-D and 3-D models this is not always true. Thus, reciprocal wave types must be calculated independently for most 2-D and 3-D structures. To "generalize" the radar patterns of the model structures, since commercial antenna have a wide variety of pulse shapes, a simple sinusoidal response having a 1.5 cycle pulse width is used.

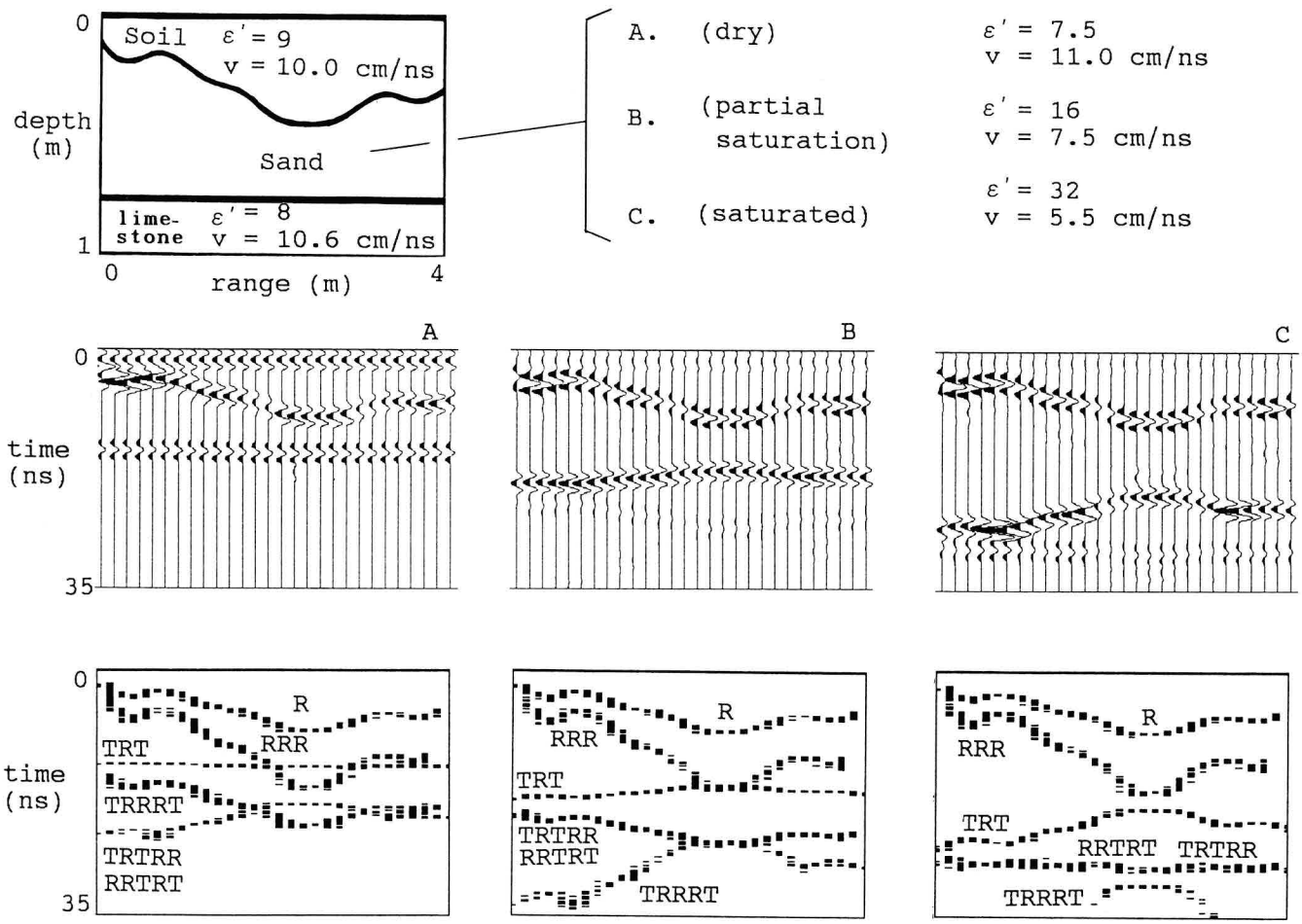

FIG. 4. Synthetic radargram simulation for a three-layer earth in which the top layer has a variable overburden thickness and the lower interface is flat. Three different dielectric permittivity values for the middle layer and their corresponding radar simulations are shown.

Simulations are computed using a 500 MHz sinusoid; a 300 MHz sinusoid is also used in one of the simulations presented.

In the model, the dielectric permittivity is held constant in the top and bottom layers. Above the top layer air ($\varepsilon' = 1, \sigma = 0$ mho/m) is assumed. In the middle layer, three dielectric permittivity values are modeled (conductivities are held constant in all cases). In model A, the dielectric values are all quite similar, so the radar images look similar to the actual ground structure. In model B, the middle layer dielectric value is increased (thereby decreasing the microwave velocity). The synthetic radargram suggests that the bottom reflecting surface is no longer flat. The reflective field strengths along the refractors are also changing. In model C, in which the velocity is about half that of the upper and lower layers, the bottom reflecting horizon becomes significantly warped because of the mapping of the upper layer thickness heterogeneities. Some of the multiple wave types also become important as the contrast changes in the middle layer. The chance of interpreting a multiple as a structural interface is also a common radargram pitfall.

A second common radargram pitfall can be easily visualized by examining how radar patterns can change significantly across structures that have only small structural differences. In Figure 5, simulated radargrams are predicted for a *V*-shaped concrete structure in which the depth to the vertex is increased. The *V*-shaped trench is filled with a simulated silt material. The contributions of the primary wave types *R*, *RR*, and *RRR* are simulated.

In model A, the *R* wave type reflection leg looks quite similar to the actual structure. The *RRR* multiple wave type can be seen in the traveltime plots. For the given contrasting materials, the multiple *RRR* is significantly lower in amplitude than *R*, but it is visible when sufficient gain is applied. The multiple *RRR* shows some "crossing" of reflection legs. This effect can be seen clearly in the direct *R* arrival for model B and model C. As the depth to the vertex increases beyond "critical," the wave type *RR* is recorded and is a significant component of the simulated GPR signal (model C). The crossing of reflections, as well as the "sudden" appearance of multiples can make radargram interpretation difficult.

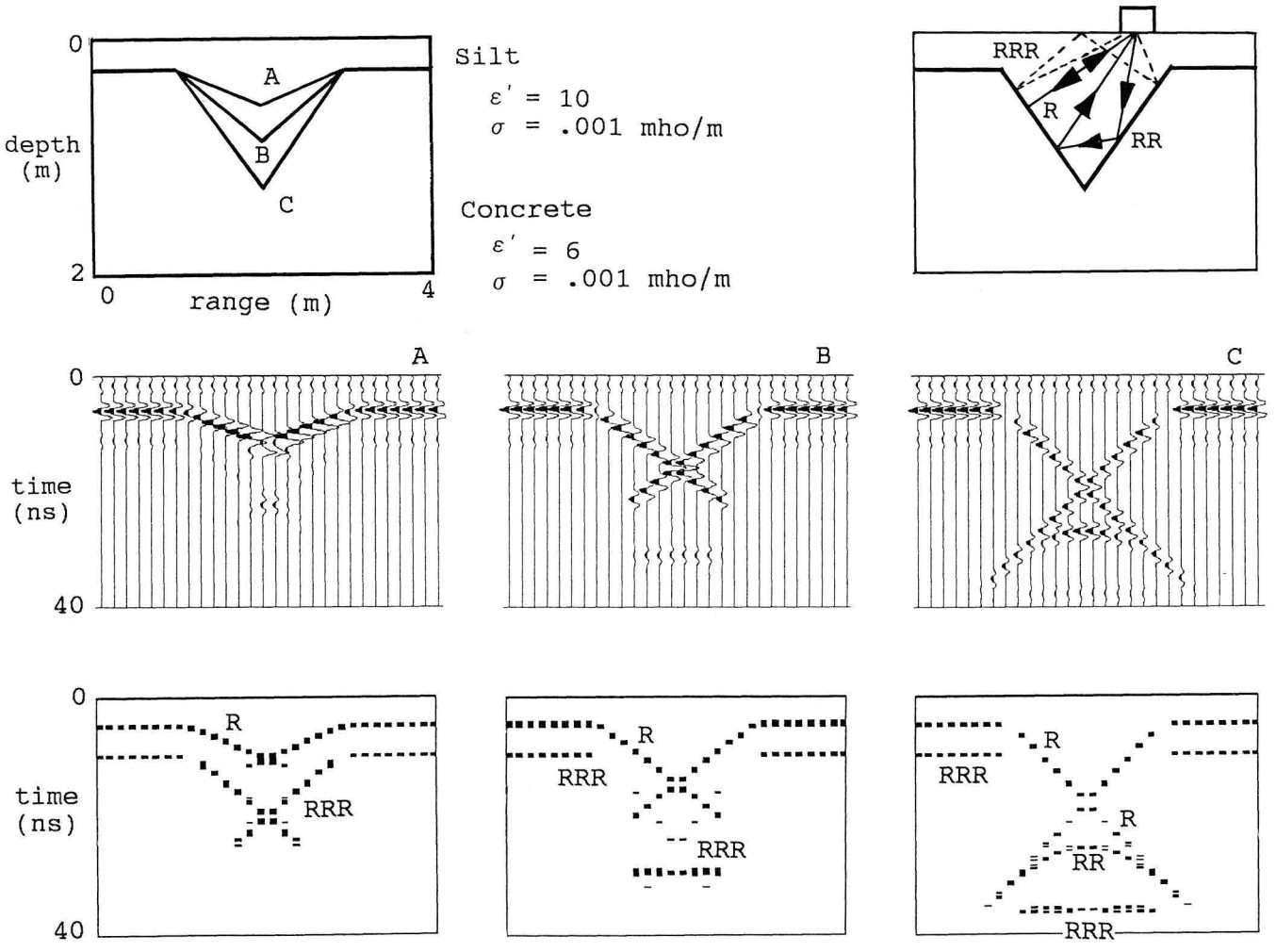

FIG. 5. GPR simulation for a series of *V*-shaped concrete trenches filled with silt material. Three different depths for the trench are examined (A = 0.55 m; B = 0.85 m; C = 1.25 m). The primary wave type contributions of *R*, *RR*, and *RRR* are computed.

Another important effect influencing GPR returns is wave refraction. Wave refraction can create broad or narrow beams depending upon the electromagnetic materials that are traversed. An example of wave refraction for real dielectric permittivity increasing from 1 to 81 and decreasing downward from 81 to 1 is shown in Figure 6. The refraction of radar waves can significantly control target cross-sections of buried objects that are imaged.

As an example, Figure 7 shows a water zone (simulating, for example, a saturated channel sand or gravel deposit—i.e., a low velocity zone) imbedded in a three-layer ground. The wave types *R*, *RR*, *RRR*, *TRT*, *TRRRT*, *TTRTT*, *TTRRTT*, *TTRRRTT*, *TRTRR*, *RRTRT*, *TTRTRRT*, and *TRRTRT* have been included in the simulation. The synthetic radargram is simulated for a 300 MHz radar antenna. The synthetic radargrams show a "lensing" effect whereby the rays are refracted downward into the low-velocity zone and arrive later in the radar scan. The low-velocity zone is found to be narrower than the actual structure when imaged with radar. The low-velocity zone causes shadow zones off to the sides, in which little or no wave energy is transmitted. Shadows can be particularly troublesome, especially if important target structures are located within them. The lensing beneath water zones is also enhanced from relatively strong recorded multiples that can traverse the (fresh) water (low velocity) zone and be recorded. (In the case of water containing some dissolved salts, the attenuation in this case would prevent strong multiples from being recorded from the water zone.)

SIMULATION IN ENGINEERING APPLICATIONS

A GPR simulation is computed for a commonly occurring engineering problem—a void beneath an "old" concrete road that may have been resurfaced. The values used for the roadbed are taken from Lau et al., (1992). In this model, the imaginary parts of the dielectric are included for added model "reality" and complexity. These values are in no way universal, as the range of electromagnetic parameters for common materials can vary significantly. Also, the electromagnetic parameters can vary with time because of changing environmental condition.

Synthetic radargram simulations are estimated beneath the resurfaced roadbed having a void (Figure 8). The synthetic shows several important features that are indicative of void spaces (high-velocity zones). At the top of the void space a phase reversal is observed. (This may not be realized, however, in the case when the void is buried in low dielectric material and is directly below high-dielectric materials). The waves traversing the void space have the appearance of warping upward since microwave velocities are highest in the void region and require the least amount of traveltime to return to the receiving antenna. Also, corner reflections within the void account for the broad hyperbolic radar reflection legs.

The simulations shown are for transmitter and receiver colocated (zero offset). The GPRSIM software package also supports data acquisition for nonzero offset reflection profiling, wide angle reflection profiling, topographic profiling,

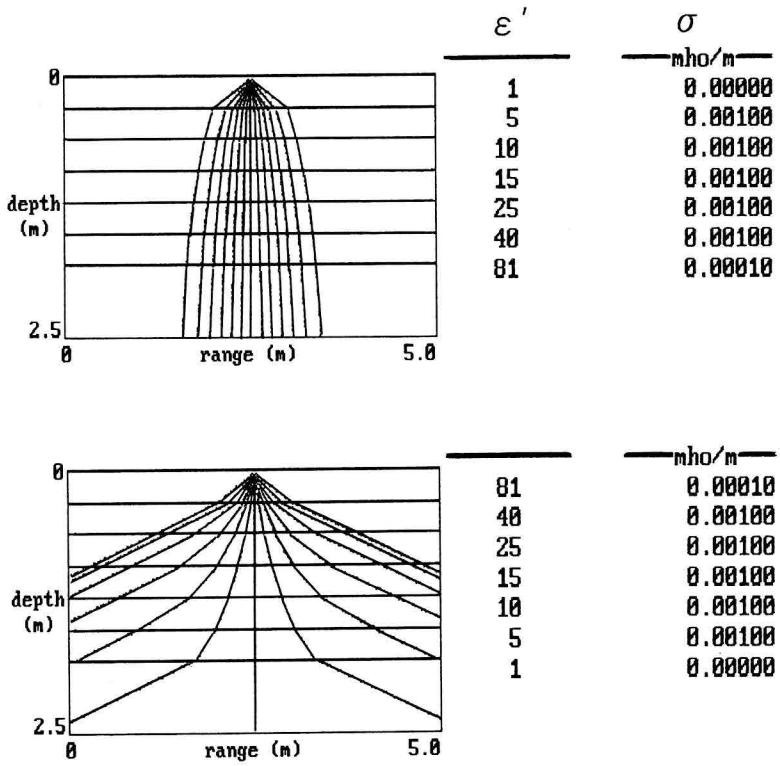

FIG. 6. The effects of wave refraction from a simulated stratigraphic structure in which the dielectric permittivity increases (top) and decreases (bottom) with depth. The starting wave angles are taken over a 120 degree directional response function (e.g., Figure 3).

and array studies. Using forward modeling, as is accomplished with the GPRSIM software, the possibility of estimating the sizes of void spaces which is crucial to road rehabilitation programs, is feasible. Voids existing beneath concrete airport runways, for example, are a particularly worrisome situation. Their detection in noisy data sets can be aided by using some forward modeling procedures.

ARCHAEOLOGICAL APPLICATION

Radar simulations at archaeological sites have been successfully applied in the study of protected burial mounds in Japan (Goodman and Nishimura, 1992, 1993). As Japanese cultural properties laws prevent the excavation of burial mounds for other than planned public construction projects on these sacred grounds, GPR is one of the most valuable tools to help learn about protected archaeological sites. One of the strongest motivations for creating synthetic radargrams are that they can quickly help to identify a class of burial styles that may exist beneath the ground. One particular style is shown in Figure 9; this type of burial, mostly found at sites that housed ancient VIPs in Japan during the Kofun period (300–700 A.D.), consists of a stone coffin-like structure. The shapes of the stone coffins are important to the archaeologist as they relate information regarding the date of construction, as well as the social hierarchy of the entombed person. Through forward modeling, a computer catalog of GPR radargram simulations similar to those in Figure 9, are being collected for a variety of different coffin structures. These catalogs of possible candidate coffin shapes will help archaeologists in their quest to determine the nature of important cultural properties buried beneath protected land.

CONCLUSIONS

The results from this study indicate it is possible to effectively model GPR signals collected over 2-D structures buried in the ground. The simulations for some simple structures also dictate the need to be careful in the interpretation of GPR radargrams as the effects of multiples, wave refraction, and geometric spreading can lead to interpreta-

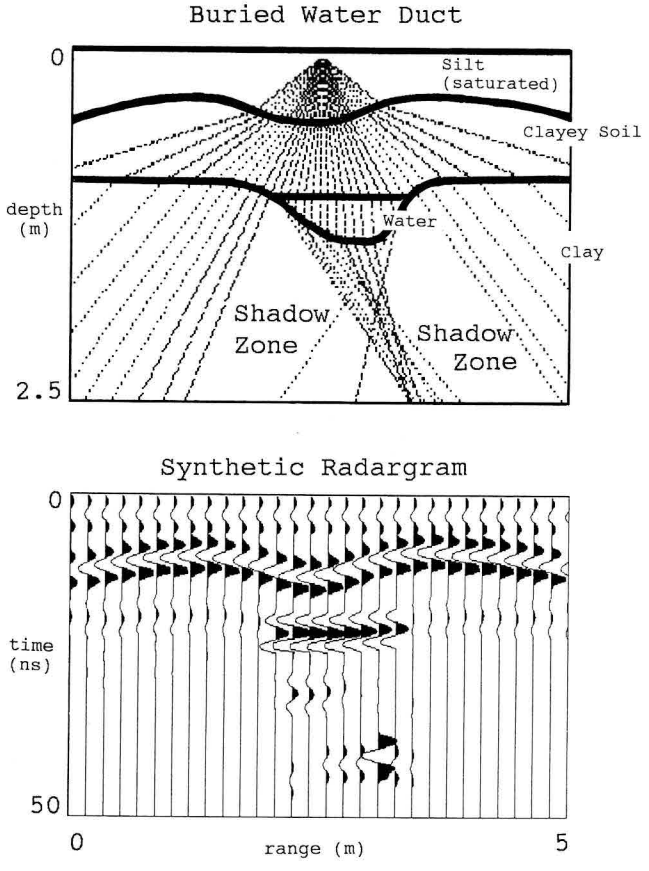

FIG. 7. GPR simulation for a three-layer ground containing an irregularly shaped subsurface water duct (low-velocity zone). Simulation is computed for a 300 MHz pulse. The wave refraction from a single antenna location is shown along with the resulting "shadow zones."

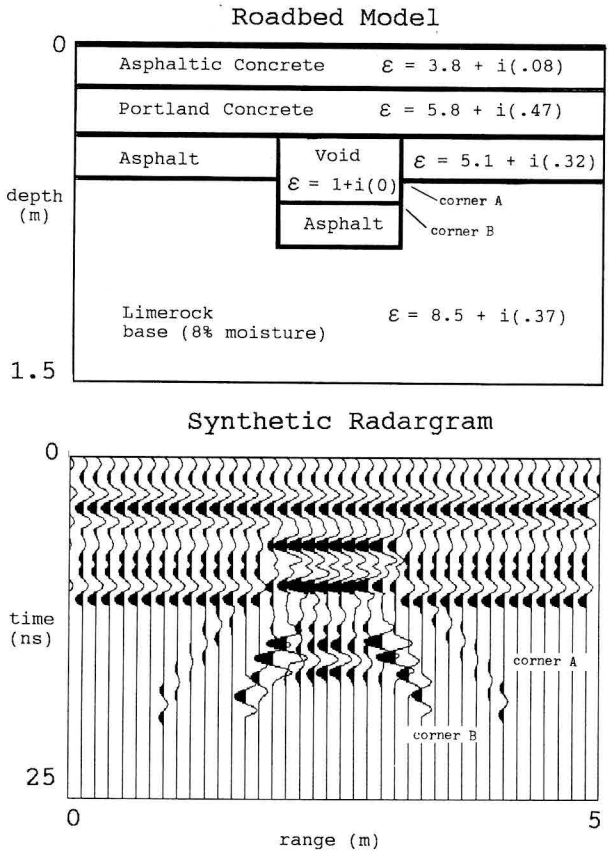

FIG. 8. Synthetic radargram simulation (500 MHz) for a four-layer "resurfaced" road containing a void space (high-velocity zone). The wave type contributions of: *R*, *TRT*, *TTRTT*, *TTTRTTT*, *RRR*, *TRRRT*, *TTRRRTT*, *TTRRTT*, *TTTRRTTT*, *TTTRRRTTT*, *RRTRT*, *TRTRR*, *TRRTRTT*, *TRTRRT* are included in the simulation. Because of the strong energy returned from recorded events of the wave type *TTRRTT*, which reflects from the corner(s) located at "A" and "B" in the model, the *TTRRTT* wave type has been identified in the synthetic radargram. The outer reflection leg of *TTRRTT* that appears as a hyperbolic pattern is from corner "A"; the inner reflection leg is primarily from within the void at corner "B."

tion pitfalls. As multichannel array surveying becomes more frequent, some of the pitfalls discussed in this study, which are found from vertical (zero offset) profiling, can be processed out of GPR radargrams. In the case of interpretation problems that can arise from changes in material properties, (e.g., Figure 4), a priori velocity information can help to determine the actual shapes of the interfaces imaged with vertical reflection profiling GPR.

This report also shows that GPR radargrams for voids beneath roadbeds can be simulated. The roadbed simulations indicate that void spaces can produce broad radar patterns caused by multiple reflections from within the void. The application of forward models that have been computed for a variety of road conditions can be used to search for a best match with field data.

The synthetic radargram method discussed, although it does not currently model diffracted waves or inhomogeneous waves, can accurately provide a close approximation to the full waveforms measured across many simple structures in the ground.

Forward modeling is essential to understanding and interpreting raw GPR radargrams and should be used in all situations when possible to add confidence in the site interpretation.

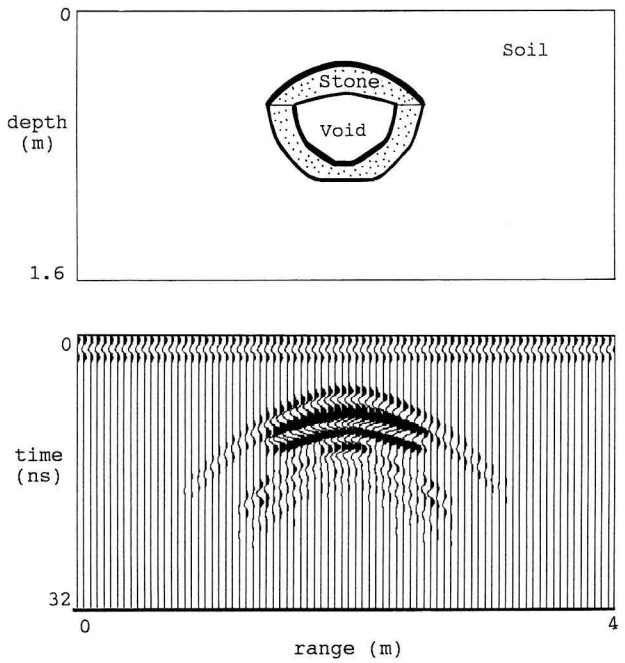

FIG. 9. GPR simulation of a generalized stone coffin commonly found at the Kofun Period (300–700 A.D.) burial mounds in Japan.

ACKNOWLEDGMENTS

The author is very grateful to the city of Nakajima Machi, Ishikawa Ken, for their support of this research. Dr. Yasushi Nishimura of the Nara National Cultural Properties Research Institute is recognized for his contributions and strong support of our small laboratory. Dr. Tokuo Yamamoto of the University of Miami helped during the initial stages of this pilot program. The Science and Technology Agency of Japan and Ishikawa Prefecture are also recognized for their contributions of the initial startup funds for this laboratory.

REFERENCES

Annan, A. P., and Davis, J. L., 1976, Impulse radar sounding in Permafrost: Radio /Sci., **11**, no. 4, 383–394.
Bevan, B., 1975, Ground-penetrating radar for historical archaeology: MASCA Newsletter, University Museum, Univ. of Pennsylvania, **11**, no. 2, 2–7.
——— 1991, The search for graves: Geophysics, **56**, 1310–1319.
Daniels, J., 1988, Locating caves, tunnels, and mines: The Leading Edge, **7**, no. 3, 32–37.
Davis, J. L., and Annan, A. P., 1989, Ground-penetrating radar for high-resolution mapping of soil and rock stratigraphy: Geophys. Prosp., **37**, 531–551.
Deen, J. K., and Feijter, J. W., 1992, Three-dimensional ground-probing radar: Finland Geol. Sur., 4th International Conference of Ground Penetrating Radar, special paper, 16, 35–40.
Duke, S., 1990, Calibration of ground-penetrating radar and calculation of attenuation and dielectric permittivity versus depth: M.S. thesis, Colorado School of Mines, T-3920.
Fisher, E., McMehan, G. A., and Annan, A. P., 1992, Acquisition and processing of wide-aperture ground-penetrating radar data: Geophysics, **57**, 494–504.
Foster, A. R., Veatch, M. D., and Baird, S. L., 1987, Hazardous waste geophysics: The Leading Edge, **6**, no. 8, 8–13.
Gassaway, G. S., Brown, R. A., and Bennett, L. E., 1987, Pitfalls in seismic amplitude versus offset analysis: case histories: Geophysics, **52**, 712.
Goodman, D., and Nishimura, Y., 1992, 2-D synthetic radargrams for archaeological investigation: Finland Geol. Sur., 4th International Conference on Ground-Penetration Radar, special paper 16, 339–343.
——— 1993, A ground-radar view of Japanese burial mounds: Antiquity, no. 255, **67**, 349–354.
Jackson, J. D., 1977, Classical electrodynamics: John Wiley & Sons, Inc.
Lau, C. L., Scullion, T., and Chan, P., 1992, Using ground-penetration radar technology for pavement evaluations in Texas, USA: Finland Geol. Sur., 4th International Conference on Ground Penetration Radar, special paper 16, 277–283.
Olhoeft, G. R., 1986, Direct detection of hydrocarbon and organic chemicals with ground-penetrating radar and complex resistivity: Proc. of the NWWA/API Conference on Petroleum Hydrocarbons and Organic Chemicals in Groundwater—Prevention Detection and Restoration, Natl. Water Well Assoc., 284–305.
Radar Handbook, 1990, Skolnik, M. I., Ed.: McGraw-Hill Book Co.
Stewart, R. D., and Unterberger, R. R., 1976, Seeing through rock salt with radar: Geophysics, **41**, 123–132.
Stove, G. C., and Addyman, P. V., 1989, Ground-probing impulse radar: An experiment in archaeological remote sensing at York: Antiquity, **63**, 337–342.
Telford, W. M., Geldart, L. P., and Sheriff, R. E., 1990, Applied geophysics: Cambridge Univ. Press.
Tucker, P. M., and Yorston, H. J., 1973, Pitfalls in seismic interpretation: SEG monograph series, **2**.
Turner, G., 1992, Propagation deconvolution: Finland Geol. Sur., 4th International Conference on Ground-penetration Radar, special paper 16, 85–93.
Ulriksen, C. P. F., 1982, Application of impulse radar to civil engineering: Ph.D. thesis, Univ. Technology, Lund, Sweden.
Vaughn, C. J., 1986, Ground-penetrating radar surveys used in archaeological investigation: Geophysics, **51**, 595–604.